16th World Congress in Computational Mechanics (WCCM)
21-26 July 2024, Vancouver, Canada
A. Korobenko, M. Laforest, S. Prudhomme, R. Vaziri (Eds)

INCOMPRESSIBLE VISCOUS FLUID ANALYSIS AROUND COMPLEX SHAPES USING ISOGEOMETRIC ANALYSIS

YUTO SAKAI[1], HIROSHI HASEBE[2] AND KAZUO KASHIYAMA[3]

[1] Graduate School of Civil, Human and Environmental Engineering, Chuo University
Kasuga 1-13-27, Bunkyo-ku, Tokyo 112-8551, JAPAN
a19.appt@g.chuo-u.ac.jp

[2] Department of Civil Engineering, Nihon University
Kanda Surugadai 1-8-14, Chiyoda-ku, Tokyo 101-8308, JAPAN
hasebe.hiroshi@nihon-u.ac.jp

[3] Department of Civil and Environmental Engineering, Chuo University
Kasuga 1-13-27, Bunkyo-ku, Tokyo 112-8551, JAPAN
kaz@civil.chuo-u.ac.jp

Key words: Isogeometric Analysis, Incompressible Viscous Flow, NURBS, Multi-Patch

Abstract. This paper aims to apply the Isogeometric Analysis(IGA) to fluid-structure interaction problem in the civil engineering field. Recently, IGA has attracted much attention as an analysis method to structure with arbitrary surfaces. In this paper, IGA is applied to a two-dimensional incompressible viscous flow problem as a basic study for the fluid-structure interaction analysis using IGA. The vortex induced vibration of a circular cylinder is investigated as a numerical example, and the effectiveness and validity of the coupled analysis using IGA are discussed.

1 INTRODUCTION

In recent years, digital fabrication technologies such as 3D printers and Computer-Aided Design (CAD) have been attracting attention in the field of civil engineering. 3D printers have the feature of being able to create any shape with a high degree of freedom from CAD data. Therefore,Isogeometric Analysis (IGA)[1][2], which has an advantage in analysis with arbitrary curved surfaces, is considered to be a very promising analysis method.

The ultimate goal of us is to develop a fluid-structure interaction analysis method with complex surfaces using IGA as an application to the civil engineering field. However, it has been difficult to represent complex geometries with single patch, and coupled analysis using it for both fluid and structure. In this study, we develop a multi-patch method based on IGA with a continuity condition[4] applied between patches for the purpose of applying IGA to complex surfaces. As an example of numerical analysis, we have conducted analysis on a fixed-supported

circular cylinder and confirmed the validity of the multi-patch method based on IGA by comparing the experimental results in terms of Strouhal number and drag coefficient. Based on the results obtained in this study, vortex excitation analysis was conducted as an example of application to fluid-structure coupled analysis, and its validity was examined.

2 NUMERICAL METHODS

2.1 Governing equations

For the governing equation of the fluid, the 2D Navier-Stokes equation described by ALE and the continuity equation is employed.

$$\rho\left(\frac{\partial \mathbf{u}}{\partial t}+\bar{\mathbf{u}}\cdot\nabla\mathbf{u}-\mathbf{f}\right)-\nabla\cdot\sigma=0 \quad in\ \Omega, \tag{1}$$

$$\nabla\cdot\mathbf{u}=0 \qquad in\ \Omega, \tag{2}$$

Where Ω is the analysis domain bounded by the boundary Γ, ρ is the density, u is the velocity vector, $\bar{u}$ is the relative velocity vector, and $\mathbf{f}$ is the body force. The stress tensor σ and the deformation rate tensor $\varepsilon\left(\mathbf{u}\right)$ are expressed as follows.

$$\sigma=-p\mathbf{I}+2\mu\varepsilon(\mathbf{u}), \tag{3}$$

$$\varepsilon(\mathbf{u})=\tfrac{1}{2}\left(\nabla\mathbf{u}+(\nabla\mathbf{u})^{T}\right), \tag{4}$$

Where p is the pressure and μ is the viscosity coefficient. The Dirichlet and Neumann boundary conditions are given by

$$\mathbf{u}=\mathbf{g} \quad on\ \Gamma_g, \tag{5}$$

$$\mathbf{n}\cdot\sigma=\mathbf{h} \quad on\ \Gamma_h, \tag{6}$$

Where Γ_g and Γ_h denote the Dirichlet and Neumann boundary conditions, respectively, and $\mathbf{g}$ and $\mathbf{h}$ are the velocity and traction on the respective boundaries. The $\mathbf{g}$ and $\mathbf{h}$ are the flow velocity and traction defined on the respective boundaries. The $\mathbf{n}$ is the outward unit normal vector.

The object is assumed to be a spring-supported two-dimensional rigid body in the flow. Its equation of motion is expressed by the following equation.

$$\mathbf{m}\ddot{\mathbf{v}}+\mathbf{c}\dot{\mathbf{v}}+\mathbf{k}\mathbf{v}=\mathbf{F} \tag{7}$$

$\mathbf{m}$ represents the mass, $\mathbf{c}$ represents the damping, and $\mathbf{k}$ represents the stiffness matrix, all of which are diagonal matrices with constant coefficients.

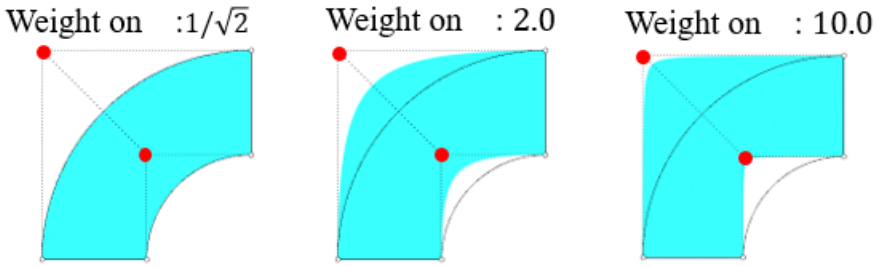

Figure 1: Weight given to control points

2.2 NURBS

In this study, the NURBS[3] is used for the shape function. As shown in **Figure 1**, the NURBS is characterized by its ability to represent various shapes with a small number of elements, depending on the weights assigned to the control points. The two-dimensional NURBS function is represented by a two-way B-spline basis function, weights assigned to control points, and position vectors of control points, where the B-spline basis function is the function defined by the Cox de Boor's gradient formula in equation (8).

If $p = 0$:

$$N_{i,0}(\xi) = 1 \qquad \text{if} \quad \xi_{\mathrm{i}} \leq \xi \leq \xi_{\mathrm{i+1}}$$
$$N_{i,0}(\xi) = 0 \qquad \text{otherwise}$$

If $p = 1, 2, 3 \cdots$:

$$N_{i,p}(\xi) = \frac{\xi - \xi_i}{\xi_{i+p} - \xi_i} N_{i,p-1}(\xi) + \frac{\xi_{i+p+1} - \xi}{\xi_{i+p+1} - \xi_{i+1}} N_{i+1,p-1}(\xi) \tag{8}$$

Where N is the B-Spline basis function in the ξ direction, i is the control point number, and p is the order of the B-Spline basis function. The ξ_i are the knots, which are the coordinates of the parameter space, given by a uniformly increasing sequence of numbers called the knot vector, as shown below.

$$\Xi = (\xi_1, \xi_2, \ldots, \xi_{n+p+1}) \tag{9}$$

The knot vector is a sequence of numbers obtained from the CAD drawn shape model and is a parameter that defines the elements in the B-Spline basis functions and IGA.

Using the B-Spline basis functions expressed in equation (8), the basis functions of the NURBS functions $R^{p,q}_{i,j}(\xi, \eta)$ and the NURBS surface $S(\xi, \eta)$ can be expressed as in equations (10) and (11).

$$R^{p,q}_{i,j}(\xi, \eta) = \frac{N_{i,p}(\xi) M_{j,q}(\eta) w_{i,j}}{\sum_{\hat{i}=1}^{n} \sum_{\hat{j}=1}^{m} N_{\hat{i},p}(\xi) M_{\hat{j},q}(\eta) w_{\hat{i},\hat{j}}} \tag{10}$$

$$S(\xi,\eta)=\sum_{i=1}^{n}\sum_{j=1}^{m}R_{i,j}^{p,q}(\xi,\eta)\,B_{i,j} \tag{11}$$

Where M is the B-spline basis function in the η direction, j is the control point number in the η direction, q is the order of the B-spline basis function in the η direction, $w_{i,j}$ is the weight assigned to the control point, $B_{i,j}$ is the position vector of the control point $B_{i,j}$ is the position vector of the control point.

2.3 Finite element method

For the governing equations (1) and (2), the following finite element equations are obtained by applying the stabilized finite element method based on the SUPG/PSPG method for the discretization in the spatial direction.

$$\begin{aligned}(\mathbf{M}+\mathbf{M}_\delta)\frac{\partial\mathbf{u}}{\partial t} &+ (\mathbf{K}(\bar{\mathbf{u}})+\mathbf{K}_\delta(\bar{\mathbf{u}}))\,\mathbf{u}\\ -(\mathbf{C}-\mathbf{C}_\delta)\frac{1}{\rho}p &+ \nu\mathbf{S}\mathbf{u}-(\mathbf{N}+\mathbf{N}_\delta)\,\mathbf{f}=0,\end{aligned} \tag{12}$$

$$\mathbf{C}^T\mathbf{u}+\mathbf{M}_\varepsilon\frac{\partial\mathbf{u}}{\partial t}+\mathbf{K}_\varepsilon(\bar{\mathbf{u}})\mathbf{u}-\mathbf{F}_\varepsilon+\mathbf{C}_\varepsilon\frac{1}{\rho}p=0, \tag{13}$$

Where $\mathbf{M}$, $\mathbf{K}$, $\mathbf{C}$, $\mathbf{S}$, $\mathbf{N}$ are the coefficient matrices, and the indices δ and ε are those due to the SUPG and PSPG terms, respectively. Also, ν denotes the kinematic viscosity coefficient. The finite element equations (12) and (13) in the fluid can be rewritten as follows.

$$\mathbf{M}\dot{\mathbf{u}}+\mathbf{K}\mathbf{u}-\mathbf{G}p=\mathbf{f} \tag{14}$$

$$\mathbf{G}^T\mathbf{u}=0 \tag{15}$$

Where $\mathbf{M}$ represents the mass matrix，$\mathbf{K}$ represents the matrix of convective and viscous terms, $\mathbf{G}$ represents the gradient matrix, and $\mathbf{f}$ represents the external forces and boundary integral terms. The variables in equations (14) and (15) are separated into components on the moving boundary Γ_I (object surface) and components elsewhere as follows.

$$\dot{\mathbf{u}}=\begin{Bmatrix}\dot{\mathbf{u}}^\alpha\\ \dot{\mathbf{u}}^\gamma\end{Bmatrix},\quad \mathbf{u}=\begin{Bmatrix}\mathbf{u}^\alpha\\ \mathbf{u}^\gamma\end{Bmatrix},\quad \mathbf{f}=\begin{Bmatrix}\mathbf{f}^\alpha\\ \mathbf{f}^\gamma\end{Bmatrix} \tag{16}$$

Where the subscript γ represents variables on the moving boundary Γ_I, and the subscript α represents others. The variables defined at the center of gravity of the object for the surface variables of the object need to satisfy the compatibility condition (17) and equilibrium condition (18) shown below.

$$\dot{\mathbf{u}}^\gamma=T^T\ddot{\mathbf{v}},\quad \mathbf{u}^\gamma=T^T\dot{\mathbf{v}}\quad\text{on}\quad\Gamma_I \tag{17}$$

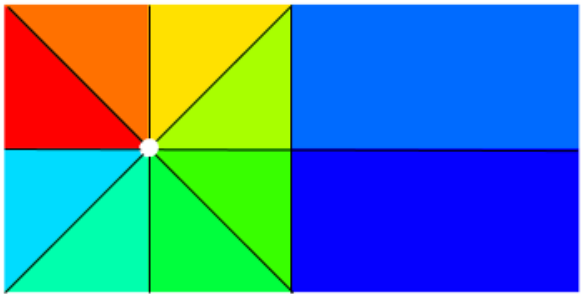

Figure 2: Patch division

$$X + T\mathbf{f}^{\gamma} = 0 \quad \text{on} \quad \Gamma_I \tag{18}$$

Regarding the finite element equations (14) and (15), by separating the components into those on the moving boundary Γ_I (object surface) and else (where the subscript γ denotes variables on the moving boundary Γ_I (object surface) and the subscript α denotes variables elsewhere), and substituting the compatibility condition of equation (17), the finite element equations become as follows.

Equation of Motion：

$$\begin{aligned} &\begin{bmatrix} \mathbf{M}^{\alpha\alpha} & \mathbf{M}^{\alpha\gamma} \\ \mathbf{M}^{\gamma\alpha} & \mathbf{M}^{\gamma\gamma} \end{bmatrix} \begin{Bmatrix} \dot{\mathbf{u}}^{\alpha} \\ T^T\dot{\mathbf{v}} \end{Bmatrix} \\ &+ \begin{bmatrix} \mathbf{K}^{\alpha\alpha} & \mathbf{K}^{\alpha\gamma} \\ \mathbf{K}^{\gamma\alpha} & \mathbf{K}^{\gamma\gamma} \end{bmatrix} \begin{Bmatrix} \mathbf{u} \\ T^T\mathbf{v} \end{Bmatrix} \\ &- \begin{bmatrix} \mathbf{G}^{\alpha} \\ \mathbf{G}^{\gamma} \end{bmatrix} \{ p \} = \begin{Bmatrix} \mathbf{f}^{\alpha} \\ \mathbf{f}^{\gamma} \end{Bmatrix} \end{aligned} \tag{19}$$

Continuity Equation：

$$\begin{bmatrix} \mathbf{G}^{\alpha T} & \mathbf{G}^{\gamma T} \end{bmatrix} \begin{Bmatrix} \mathbf{u}^{\alpha} \\ T^T\mathbf{v} \end{Bmatrix} = 0 \tag{20}$$

Find the nodal force f^{γ} on the object surface from the second line of equation (19). Also, the equilibrium condition equation (18) and substituting it into the equation of motion of the object, we obtain

$$\mathbf{m}^*\ddot{\mathbf{v}} + \mathbf{c}^*\dot{\mathbf{v}} + \mathbf{k}\mathbf{v} = -T\left(\mathbf{M}^{\gamma\alpha}\dot{\mathbf{u}}^{\alpha} + \mathbf{K}^{\gamma\alpha}\mathbf{u}^{\alpha} - \mathbf{G}^{\gamma}p\right) \tag{21}$$

Where

$$\mathbf{m}^* = \mathbf{m} + T\mathbf{M}^{\gamma\gamma}T^T, \quad \mathbf{c}^* = \mathbf{c} + T\mathbf{K}^{\gamma\gamma}T^T$$

This means that the mass $\mathbf{m}$ and damping $\mathbf{c}$ of the object are added to the additional mass and damping effects of the coupling with the surrounding fluid, respectively. The first line of equation (19) shows the equations of motion of the fluid with respect to nodes other than the object surface nodes.

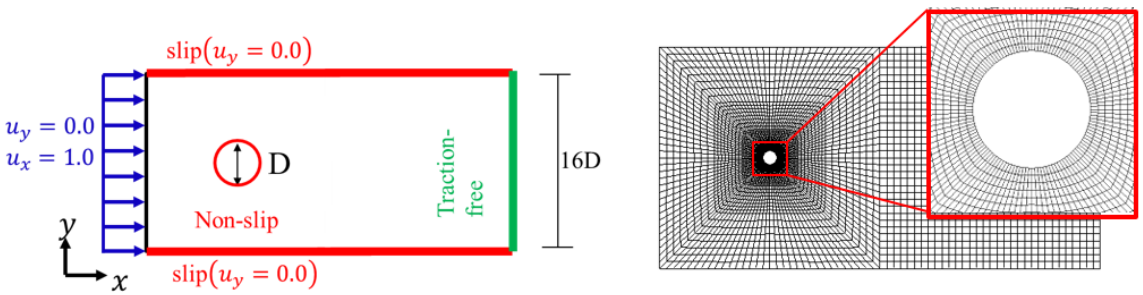

(a) Analysis Model (b) Analysis Mesh

Figure 3: (a) Analysis Model (b) Analysis Mesh

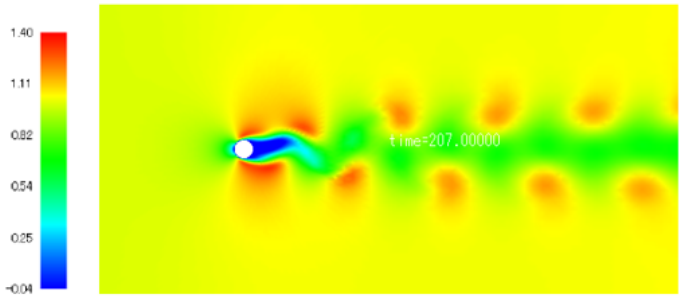

Figure 4: Flow direction velocity visualization

2.4 Multi-Patch Method

Multi-patch method was applied. In this method, the geometry is represented by multiple NURBS surfaces, and each patch has its own shape and geometrical characteristics, which is expected to increase the degree of freedom of geometry representation and the accuracy of analysis.

In this study, a multi-patch analysis is performed by applying a continuous condition of Matrix-Vector superposition between patches. The analysis is performed with 10 patches, and the patch division is shown in **Figure 2**.

3 NUMERICAL EXAMPLES

As numerical examples, flow analysis around a two-dimensional cylinder and vortex excitation analysis are shown.

3.1 Analysis of a fixed-supported cylinder

The stiffness matrix of the spring multiplier is set to be infinite, and the flow around a two-dimensional circular cylinder is analyzed. The validity of the IGA fluid analysis method based on the multi-patch method is verified.

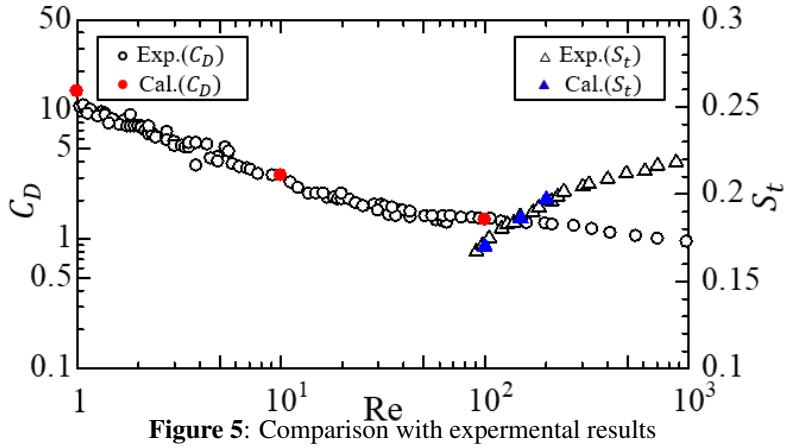

Figure 5: Comparison with expermental results

3.1.1 Numerical conditions

The analytical model and mesh are shown in the **Figure 3(a)**, **Figure 3(b)**. The analysis was performed with 6120 total control points, 4096 total elements, and 10 patches. As boundary conditions, no-slip condition is applied on the surface of the cylinder and the traction-free condition is applied at the downstream outlet boundary. The Reynolds number is set to 10^n (n=0,2) and the time increment δt is set to 0.01.

3.1.2 Numerical results

As an example of the results, the visualization results of the velocity in the flow direction at Reynolds number 100 at dimensionless time T=207, when the lift coefficient is maximum, are shown in **Figure 4**. From these results, it is confirmed that IGA can be used to analyze the flow around a circular cylinder and that periodic Kalman vortex sequences are generated.

Next, the average values of drag coefficient for each Reynolds number and Strouhal number are compared with the experimental results[5] (T=200 to 300) in **Figure 5**. The figure shows that the results of the analysis are in good agreement with the experimental results, which confirms the validity of the results in the analysis using IGA based on the multi-patch method.

3.2 Analysis of Elastically Supported Cylinder

As a second example of analysis, vortex excitation analysis of a circular cylinder is performed. The analytical model is based on the experiment in which Anagnostopoulos and Bearman[6] succeeded in capturing the lock-in at a flow of Reynolds number about 110. The cylinder is assumed to be rigid, and the analysis is performed for a spring-supported one-degree-of-freedom system.

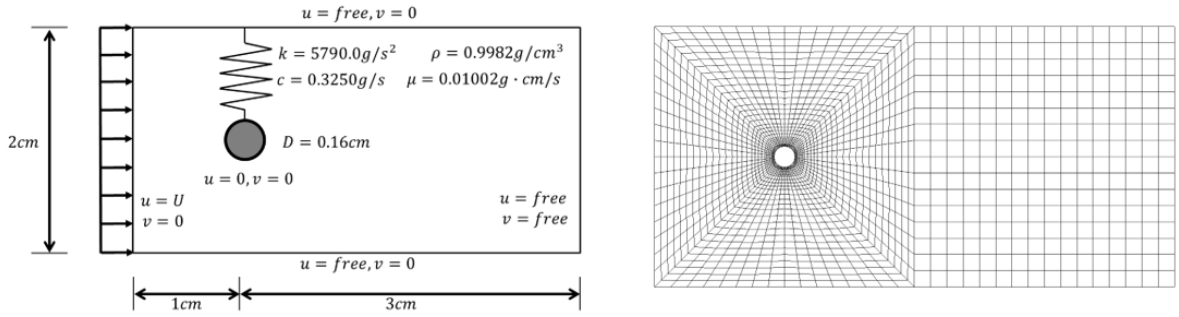

(a) Analysis Model (b) Analysis Mesh

Figure 6: (a)Analysis model (b)Analysis mesh

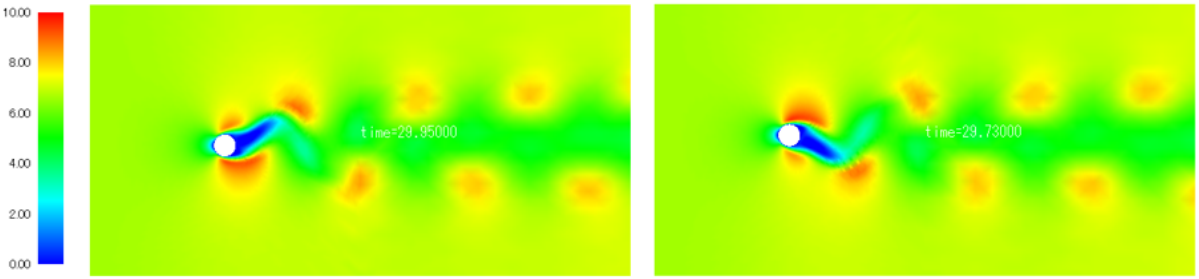

a) Flow direction velocity (T=29.95[s]) b) Flow direction velocity (T=29.73[s])

Figure 7: Flow direction velocity visualization

3.2.1 Numerical conditions

The analytical model and various analytical conditions are shown in **Figure 6(a)**. The no-slip condition on the surface of the cylinders, the slip condition on the side, and the traction-free condition on the outlet boundary are applied.

By changing the upstream velocity as the inflow condition, analysis was performed with multiple Reynolds numbers. As shown in **Figure 6(b)**, the analysis mesh has 10 patches with 2760 control points and 2048 elements.

3.2.2 Analysis results

The visualization results of flow direction velocity (Re=105) are shown in **Figure 7**. a) is the visualization result at time T=29.95[s] when A/D is the lergest and b) is the visualization result at time T=29.73[s] when A/D is the smallest. From these results, it can be seen that the Karman vortex sequence is generated and the cylinder is moving under the influence of the flow.

Next, the representative time history waveforms of the cylinder displacement from Re=90 to

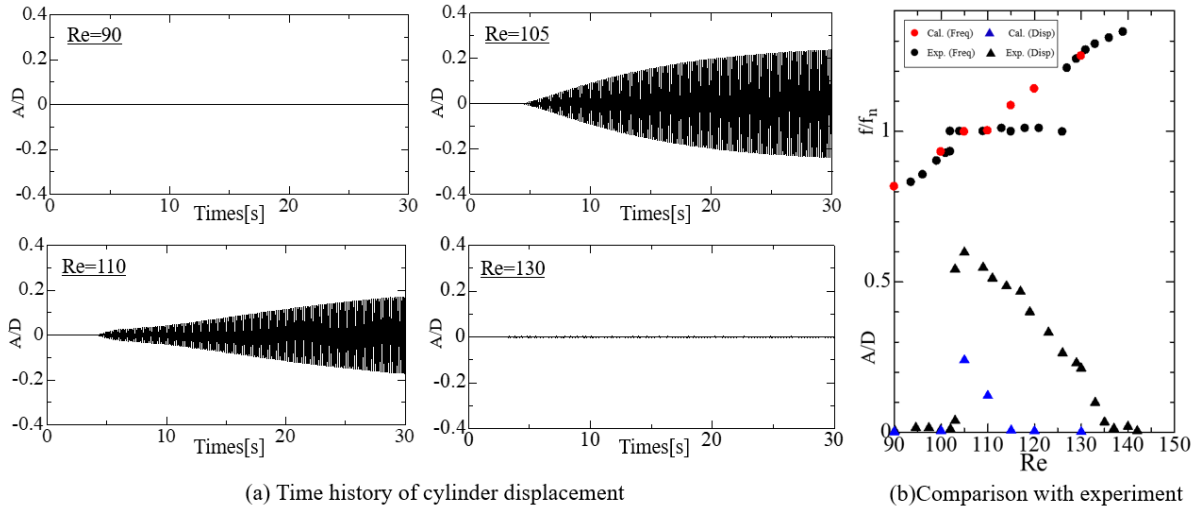

(a) Time history of cylinder displacement (b)Comparison with experiment

Figure 8: (a) Time history of cylinder vibration (b) Comparison with expermental results

Re=130 are shown in **Figure 8(a)** and the oscillation amplitude and vortex shedding frequency of the cylinder at several Reynolds numbers and a comparison with experimental results are shown in **Figure 8(b)**. Where A is the amplitude of the cylinder, D is the diameter of the cylinder, f is the vortex emission frequency, and f_n is the natural frequency of the cylinder. These results show that the vortex shedding frequency is in good agreement with the experimental solution. Although the analytical results for the amplitude show differences from the experimental values, the lock-in phenomenon, in which the displacement of the cylinder increases in the region where the vortex shedding frequency and the natural frequency of the cylinder coincide, can be confirmed.

4 CONCLUSIONS

In this paper, we investigated a divelopment of a fluid-structure interaction method based on IGA for incompressible viscous flow problem. In order to investigate the validity of present method, we applied the method to a two dimentional flow problem around a circular cylinder. The following conclusions are obtained.

- A multi-patch method using IGA is developed and the validity of the results in the analysis of flow around a cylinder is confirmed.
- We were able to catch the lock-in phenomenon around Reynolds number 105 and confirmed the resonance phenomenon caused by it.
- The amplitude of the cylindrical vibration is different from the experimental value, and further investigation is required.

As future work, we plan to improve the accuracy of the cylindrical amplitude analysis and to conduct an analysis using elastic bodies in the structure.

REFERENCES

[1] T.J.R.Hughes, J.A.Cottrell and Y.Bazilevs, Isogeometric analysis: CAD, finite elements, NURBS, exact geometry and mesh refinement, Computer Methods in Applied Mechanics and Engineering, Vol.194, pp.4135-4195, 2005.

[2] J.A.Cottrell, T.J.R Hughes and Y.Bazilevs, Isogeometric analysis: Toward integration of CAD and FEA, *Wiley Publishing*, 335p, 2009.

[3] L.Piegl, W.Tiller, The NURBS book 2nd edition, *Springer Science & Business Media*, 1996.

[4] S.Fujima, Y.Fukasawa and M.Tabata, Finate element formulation of periodic conditions and numerical observation of three-dimensional behavior in a flow, 1993.

[5] R.L.Panton, Incompressible flow, *John Wiley & sons Inc.*, 1995.

[6] P.Anagnostopoulos, P.W.Bearman, Response characteristics of a vortex-excited cylinder at low Reynolds number, *Journal of Fluids and Structures*, Volume 6, pp39-50, 1992.